JACS
JOURNAL OF THE AMERICAN CHEMICAL SOCIETY

pubs.acs.org/JACS

Article

Protein Binding and Orientation Matter: Bias-Induced Conductance Switching in a Mutated Azurin Junction

Jerry A. Fereiro,* Tatyana Bendikov, Israel Pecht, Mordechai Sheves,* and David Cahen*

Cite This: *J. Am. Chem. Soc.* 2020, 142, 19217−19225

Read Online

ACCESS | Metrics & More | Article Recommendations | Supporting Information

ABSTRACT: We observe reversible, bias-induced switching of conductance via a blue copper protein azurin mutant, *N42C Az*, with a nearly 10-fold increase at |*V*| > 0.8 V than at lower bias. No such switching is found for wild-type azurin, *WT Az*, up to |1.2 V|, beyond which irreversible changes occur. The *N42C Az* mutant will, when positioned between electrodes in a solid-state Au−protein−Au junction, have an orientation opposite that of *WT Az* with respect to the electrodes. Current(s) via both proteins are temperature-independent, consistent with quantum mechanical tunneling as dominant transport mechanism. No noticeable difference is resolved between the two proteins in conductance and inelastic electron tunneling spectra at <|0.5 V| bias voltages. Switching behavior persists from 15 K up to room temperature. The conductance peak is consistent with the system switching in and out of resonance with the changing bias. With further input from UV photoemission measurements on Au−protein systems, these striking differences in conductance are rationalized by having the location of the Cu(II) coordination sphere in the *N42C Az* mutant, proximal to the (larger) substrate-electrode, to which the protein is chemically bound, while for the *WT Az* that coordination sphere is closest to the other Au electrode, with which only physical contact is made. Our results establish the key roles that a protein's orientation and binding nature to the electrodes play in determining the electron transport tunnel barrier.

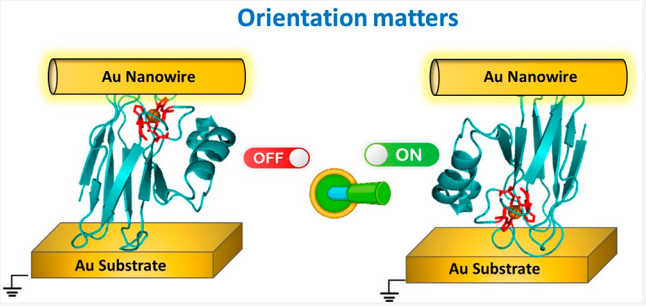

INTRODUCTION

Proteins integrated into nanoscale devices as charge transport material may provide a route to future bioelectronic applications.[1,2] The functions of such applications would rest fundamentally on charge transport via the proteins and across the interface between them and the electrodes.[3] Bioelectronic devices such as logic gates[4] and multistate memory devices[5] using *redox* proteins as building blocks have already been reported. We have recently explored the possibility of using monolayers of redox proteins in an essentially dry state, to achieve transistor action[6] with azurin, or conductance switching[7] with a cytochrome *c* mutant. We now succeeded in observing switching also with an azurin mutant, a step toward multifunctional protein electronics.

Azurin (Az) is an electron transfer copper protein involved in the energy conversion system of the bacterium *Pseudomonas aeruginosa*.[8,9] The copper ion[10] is bound at one ("north") end of the barrel-shaped protein, coordinated to three equatorial ligands (N of His46 and His117 and S of Cys112) and two weaker bonded axial ligands (S of Met121 and the peptide backbone oxygen of Gly45), resulting in a distorted trigonal bipyramidal geometry[9,11] (cf. Figure 1A). A single disulfide bridge located at the other, "south", end of the protein connects residues Cys3 and Cys26 in a disulfide bridge. Az structure and function were found to be maintained upon adsorption on surfaces in an essentially dry state.[12] This, along

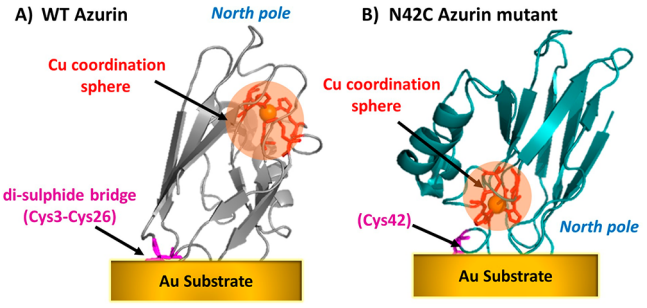

Figure 1. (A) Schematic structure of the substrate-attached *WT Az* (PDB file 1azu); the Cu(II) coordination sphere is presented in an orange sphere; the coordinating residues are shown as red sticks. (B) As A, but for the *N42C Az* mutant.[25] Asparagine 42 was replaced by cysteine (shown in violet), which served to form a Au−S bond. The violet in A now denotes the two cysteine residues that were replaced by alanines in *N42C Az*.

Received: August 21, 2020
Published: November 3, 2020

https://dx.doi.org/10.1021/jacs.0c08836
J. Am. Chem. Soc. 2020, 142, 19217−19225

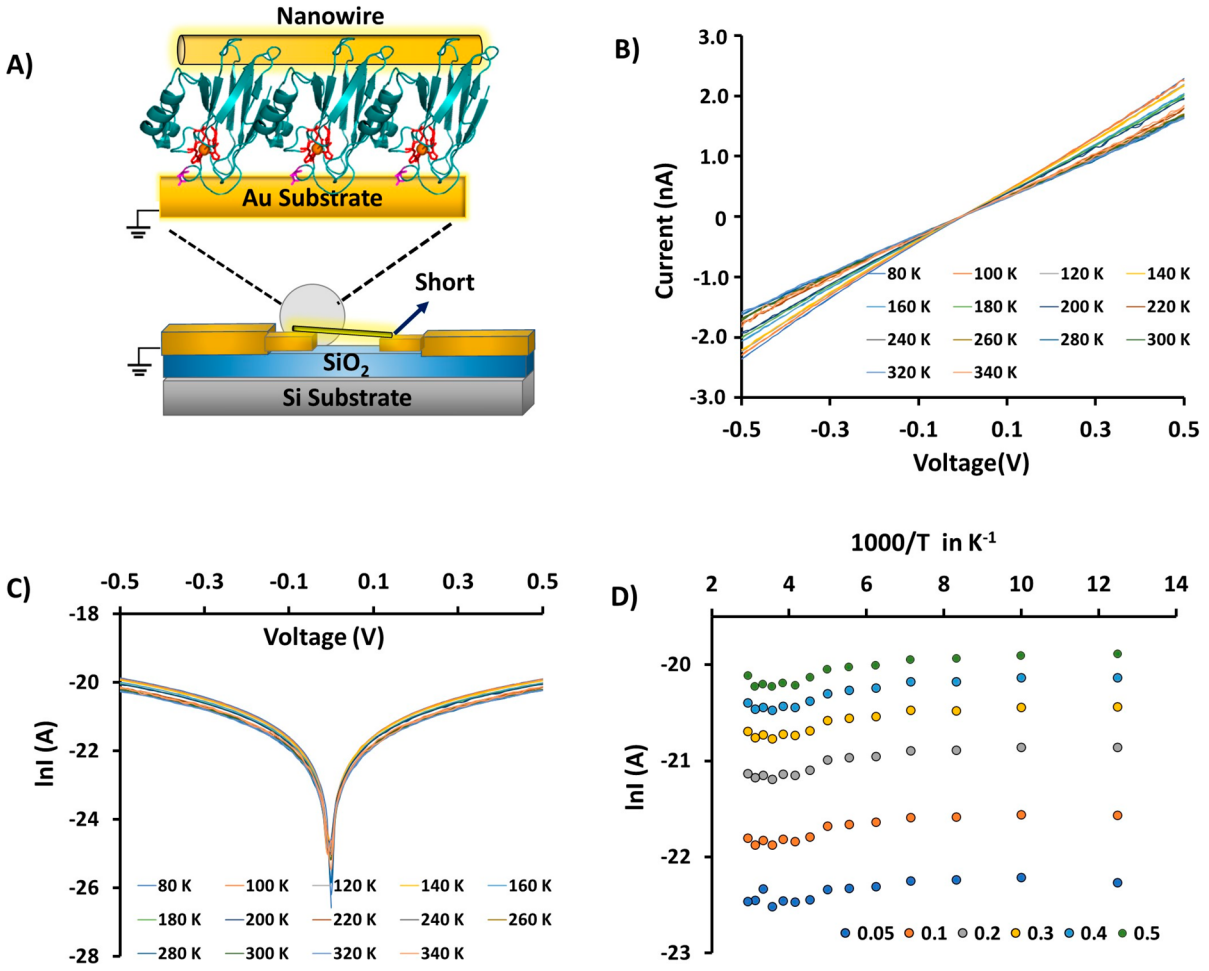

Figure 2. (A) Schematic illustration of the solid-state protein junction, prepared by nanowire trapping, for charge transport measurements. Inset shows the structure of *N42C Az*, with the same color code as in Figure 1. (B) Current−voltage (*I*−*V*) plots and (C) corresponding ln(current)−voltage (*ln*I−V) plots of the Au−*N42C Az*−Au junction at temperatures, *T*, between 80 and 340 K. (D) ln(current) at 50−500 mV applied bias voltages, as a function of 1000/*T*, for the *N42C Az* junctions.

with its proven robustness,[13,14] has made Az a very promising candidate for bioelectronic applications.

Conductance via Az in aqueous solution has been measured by various techniques[15−18] including electrochemical scanning tunneling microscopy (EC-STM).[15] All current−voltage[19,20] and current−distance spectroscopy[21] studies, carried out on Az, established the important role that the Cu(II) redox site plays in the electron transport (ETp) process.

Previously, we have investigated ETp via solid-state junctions of wild-type (WT) Az monolayers in the Au−Az−Au configuration. Weakening the electronic protein−electrode coupling by inserting a hydrocarbon spacer molecule between Az and one of the (Au) electrodes, while the other Au substrate is contacted by an Au−S bond to the protein,[18] changed the ETp mechanism from OFF-resonant tunneling (without spacer), to ON-resonant tunneling (with spacer).[18] Further, by chemically modifying the spacer−protein interaction (using *WT Az* junctions with a spacer molecule), it was possible to change the frontier orbitals' energies.[22] In all these studies *WT Az* was bound to the Au electrode−substrate by an Au−S bond, formed with one of the cysteines at the south pole, that forms the above-mentioned Cys3−Cys26 disulfide bridge, which cleaves spontaneously when Az contacts the Au surface. Consequently, the north end of Az, the side with the Cu(II) coordination shell, is proximal to the other electrode (or to any molecule, bound to that electrode). Thus, *WT Az*−electrode coupling by covalent bonding occurs at its redox-inactive end, while interaction proximal to the redox-active side is noncovalent. As coupling to the electrodes appears to dominate the ETp efficiency of proteins,[23] the results obtained so far raise the question of how far the location of the covalent Az−electrode bond and the protein's relative orientation with respect to the electrodes affect conductance via Az junctions. Obviously, the answer to these questions is rather crucial for designing future protein-based electronics.

We address here these questions by using the Az mutant *N42C Az*, where the two native disulfide bridge-forming cysteine residues (3 and 26) are replaced by alanines, and the native asparagine residue 42 is replaced by a cysteine.[24,25] Position 42 is proximal to the Cu(II) site (cf. Figure 1B), enabling the study of ETp via an Az bound to the electrode at a very different protein locus and in an orientation that is nearly opposite that of *WT Az* in the hitherto studied junctions. In this study we provide compelling evidence for the importance of a protein's orientation, with respect to the electrodes in a junction, for controlling its conductance. We find experimentally that orientation enables increasing the conductance of a well-known protein junction by ∼10 times, allowing its use as a switch. Such a result has so far rarely been observed in the field of solid-state bioelectronics. Furthermore,

https://dx.doi.org/10.1021/jacs.0c08836
J. Am. Chem. Soc. 2020, 142, 19217−19225

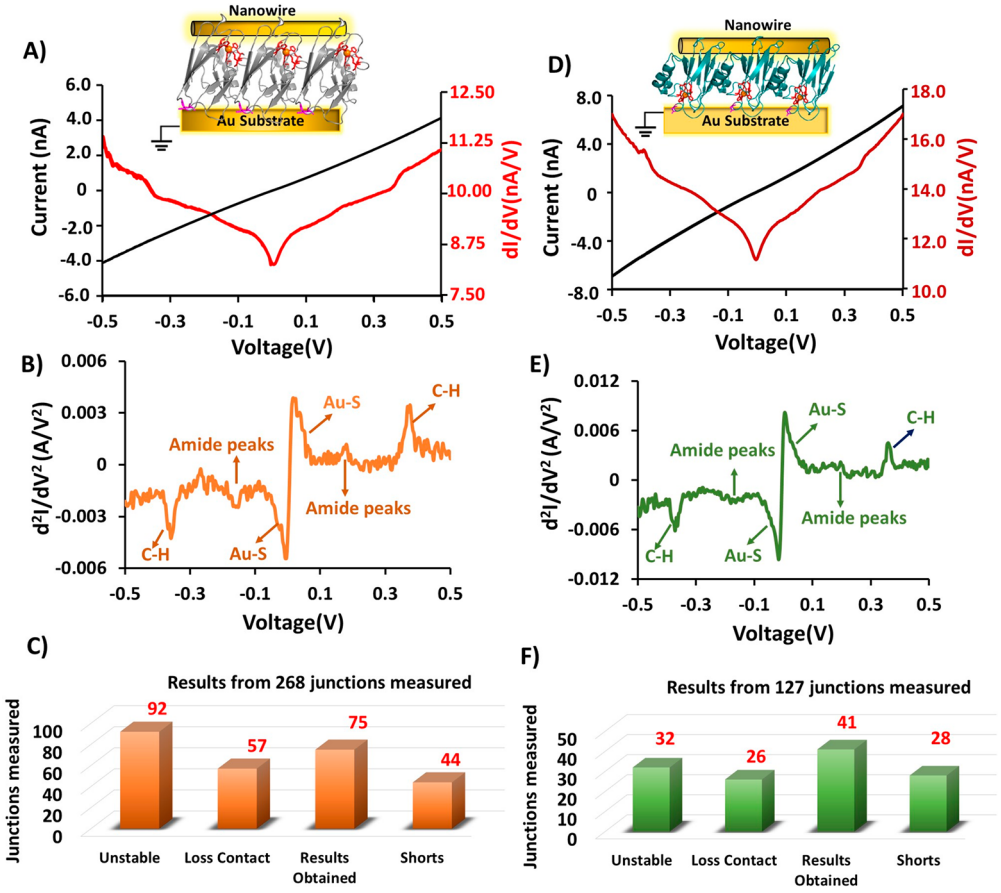

Figure 3. (A, top left) Current−voltage, $I-V$ (black), and conductance−voltage, $(dI/dV)-V$ (red), plots via the *WT Az* junction between −0.5 and +0.5 V. (B, middle left) IETS, $(d^2I/dV^2)-V$, of the same junction. (C, bottom left) Results statistics of the *WT Az* junctions used in this study. (D, E, F) As A, B, C, but for the *N42C Az* junctions. All data presented here are from experiments done at 10−15 K.

we provide an *experimental* photoemission-based, energy level interpretation of the switching behavior between the two different protein orientations. Our results suggest a novel strategy to regulate conductance switching by use of protein−electrode orientation and its control.

EXPERIMENTAL SECTION

Materials. *Az Mutant.* Protocols of production and purification of the *WT Az*[26,27] and the mutated *N42C Az*[24] have been published (see SI). Briefly, in the latter, triply mutated Az, cysteine residues 3 and 26 were replaced by alanines and a cysteine replaced the native asparagine residue 42. In the presence of oxidants such as ferricyanide or even dioxygen the mutant forms dimers where two *N42C Az* monomers are covalently bound by a disulfide bridge, between the Cys 42 in each one (see SI, Figure S1).[25] The *N42C Az* mutant's three-dimensional structure has been determined, and several detailed studies have examined and established its stability.[25,28−30]

A mutation made at the secondary Cu(II)-coordination sphere of the copper may change the Cu electronic state, which, in turn, can affect the charge transport properties.[15] In the case of the *N42C Az* mutant, the mutation ("N" to "C" at position 42), though proximal to the Cu, is not in the secondary Cu(II)-coordination shell and, therefore, does not affect the Cu(II) electronic state. Experimentally, this is shown by the finding that the typical LMCT band of the type 1 Cu(II) site, centered at ∼630 nm, of the *N42C Az* mutant overlaps with that of the *WT Az* (see SI, Figure S4).

Junction Fabrication and Monolayer Formation. Junction fabrication, formation of mutated Az monolayers, and their characterization were carried out following previously published procedures.[18,22,31]

When the Az mutant's solution contacts the lithographically fabricated μm-sized Au electrode, the dimer's disulfide bridge (Cys 42−Cys42) is cleaved and the *N42C Az* monomer becomes covalently bound to Au via its exposed Cys 42 thiolate (see Figure 1B). Formation of the *N42C Az* mutant monolayers on the Au surface was confirmed, and their properties were characterized by ellipsometry (from which an optical thickness of 20−22 Å is deduced, comparable to that found for monolayers of *WT Az*), AFM (topography, see Figure S10 in SI), and UV−vis and PM-IRRAS spectroscopies (see SI, Figures S3 and S6). The observed N 1s, C 1s, O 1s, and S 2p peaks in the XPS spectra of Au surfaces, modified by *N42C Az* adsorption, qualitatively confirm formation of the *N42C Az* monolayers on the Au surface; the binding energy of the S $2p_{3/2}$ peak maximum at around 162 eV confirms the formation of Au−S bonds (for more details see SI, Figure S5).

The "suspended-wire" technique[32−34] was used to form the protein's top electrical contact. In this method's protocol individual Au nanowires (NWs) are electrostatically trapped between pairs of lithographically prepared Au electrodes (see Figure 2A). Thereby a junction forms between the *N42C Az* monolayer on one of the Au electrodes and the electrostatically trapped single Au nanowire (see Figure 2A, as shown elsewhere[31] in this method the trapping always shorts the other electrode). The Au-bound *N42C Az* mutant monolayers were shown to be sufficiently robust for solid-state electron transport measurements from room temperature down to cryogenic (∼10−15 K) ones and back.

RESULTS

The ETp via *WT Az* and *N42C Az* Is Temperature Independent. Figure 2A illustrates schematically the structure of the Au−*N42C Az*−AuNW (Az−Au nanowires)

https://dx.doi.org/10.1021/jacs.0c08836
J. Am. Chem. Soc. 2020, 142, 19217−19225

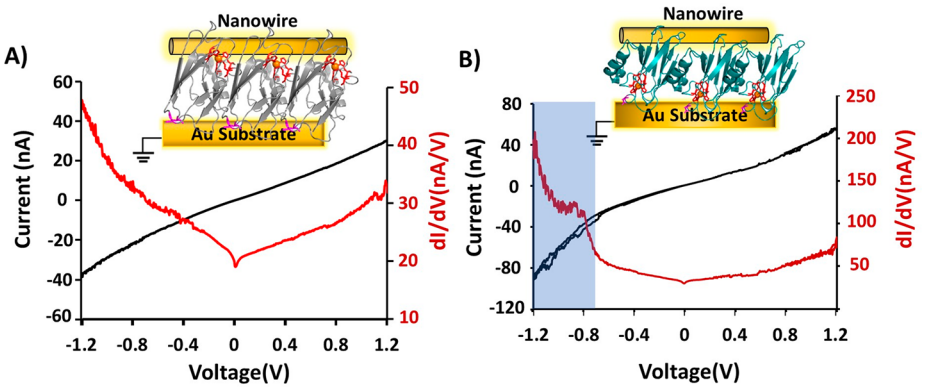

Figure 4. (A) Current−voltage (I−V, black) and conductance voltage (dI/dV−V, red) plots of measurements via the *WT Az* junction between −1.2 and +1.2 V. (B) As A, but for the *N42C Az* junction. Both experiments were carried out at 15 K.

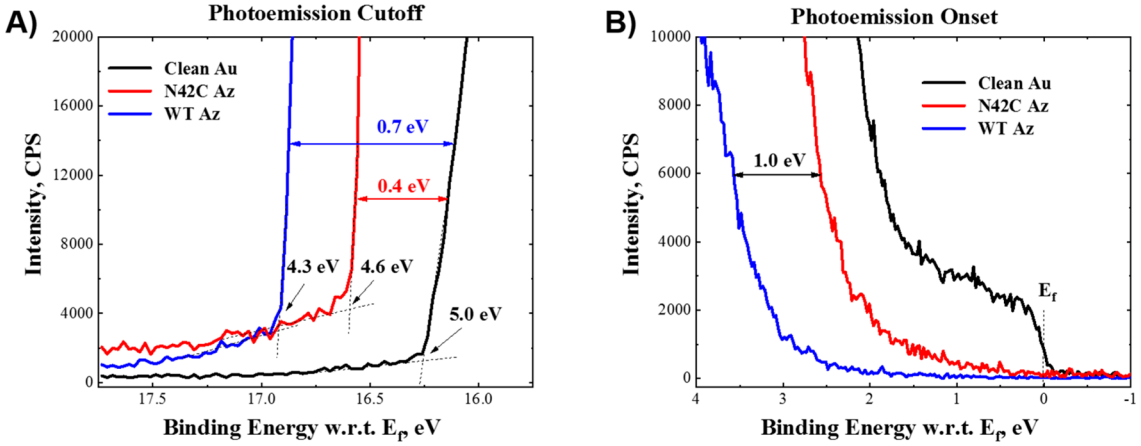

Figure 5. (A) Close-up of the secondary electron photoemission cutoff (SEPC) region of the three studied surfaces, viz., clean Au, Au with an *N42C Az* monolayer, and Au with a *WT Az* monolayer, from which the work function values are derived. (B) Zoom-in of the UPS spectra near the Fermi level (linear intensity scale), showing E_{HOMO} for the three studied surfaces, for clean Au $E_{HOMO} = E_f$. Use of log(intensity) yields similar differences in onset energies between *WT* and mutant Az, but shifted ∼1.5 eV toward 0 eV, i.e., E_f (see SI, Figure S12). The complete He I and He II spectra are shown in the SI (Figure S13).

junction configuration employed in this study. All the results were obtained in the two-wire mode, where the AuNW is biased and the bottom Au substrate is electrically grounded. Current−voltage characteristics were measured, using this configuration, in the 80−340 K temperature range with 20 K intervals (Figure 2B). Results were comparable to those obtained earlier for *WT Az*,[18] notwithstanding the differences in the protein's site of binding and orientation between the electrodes. Figure 2C presents the ln(current)−voltage plots corresponding to Figure 2B. Figure 2D presents the ln(current) vs 1000/T(temperature) plots at positive bias voltages from 50 to 500 mV. The measurements at negative bias voltages gave similar results (see SI, Figure S11). The relatively small, <∼50%, nonmonotonic changes (see Figures 2D and S11) over the whole temperature range can be ascribed to differences in thermal expansion between the electrodes and substrate, and of the protein monolayer. Thus, taking into consideration the fluctuations in the results, it is possible to conclude that *temperature-independent* ETp is observed. Such a behavior is consistent with charge transport by way of quantum mechanical tunneling. The observed temperature-independent ETp is similar to that observed for *WT Az*,[20,35] a behavior that we found recently to persist down to 4 K.[34]

Conductance and Inelastic Electron Tunneling Spectroscopy, IETS, Measurements. Together with the current, we *measured* simultaneously the conductance (dI/dV) and the conductance derivative (d^2I/dV^2 − V), all as a function of the applied voltage. The last type of data, IETS, provides the vibrational energies of the conducting medium, reflecting the inelastic part of the electron transport across the junction. Figure 3A and D present I−V and dI/dV−V curves for *N42C Az* and *WT Az*, illustrating similar ETp behavior of both proteins at <0.5 V bias. The small kinks observed in the dI/dV−V plots (Figure 3A and D) reflect the opening of inelastic conduction channels at voltages corresponding to the energies of vibrational modes. The dip near zero bias is attributed to the large number of low-energy vibrations in the complete junction (i.e., including the electrodes). The peak in the IETS spectrum (d^2I/dV^2 − V) (Figure 3B and E) observed at around 0.37 V (3000 cm^{-1}) is attributed to the C−H stretching mode, and the peaks at 0.20/0.18 V (1640/1520 cm^{-1}) to the amide I and amide II bands.[31] Comparison of Figure 3B and E shows that at <0.5 V bias the IETS spectra for *N42C Az* and *WT Az* are similar. Thus, over this bias range, changing the protein's bonding to and orientation between the electrodes, including the protein surface region near the covalent bond to one of the electrodes, do not affect the ETp across these junctions.

To explore whether this similarity is maintained at higher bias, I−V curves and conductance−voltage plots were measured for both types of protein junctions at >|0.5| V. We

https://dx.doi.org/10.1021/jacs.0c08836
J. Am. Chem. Soc. 2020, 142, 19217−19225

note that measurements at such high bias should be done with great care, because the high electric field strength (>∼1G V/m, neglecting the voltage drop across contact leads) can lead to instabilities and irreversible changes in the protein structure.[36] Figure 4B presents an overlay of the $I-V$ and $dI/dV-V$ plots of *N42C Az* mutant junctions. In the high negative bias range (blue shading in Figure 4B) a distinctly different behavior from that in any other examined voltage range is observed. This different behavior is clearest in the $dI/dV-V$ plot. The conductance shows only very minor changes until −0.5 V, but increases up to 3-fold at −0.8 V, followed by a slight decrease before increasing even further. The conductance switch observed in N42C Az junctions increases up to 10-fold (see SI, Figure S8B). No such behavior is observed for the current (Figure 4A, black line) or conductance via *WT Az* (Figure 4A, red line) up to 1.2 V.

The conductance−voltage results presented in Figure 4A and B can be a result of differences between *WT Az* and *N42C Az* in cross-junction energy level profiles. Thus, applying a sufficiently high (absolute) bias (without damaging the junction) shifts one of the frontier energy levels of *N42C Az* into the applied bias window of the junction (see Figure 6H), thereby inducing a resonance between the energy levels. In contrast, for the *WT Az* junction, the absence of peaks in the $dI/dV-V$ plot at high bias reflects that their frontier orbital energy levels are too far energetically from the Fermi level to reach resonance conditions (see Figure 6D). The broadening of the shoulder/peak in Figure 4B (red line), at ∼12 (±3) K, is consistent with the notion that more than one energy level is in the Fermi window over this −0.8 to −1.0 V range.

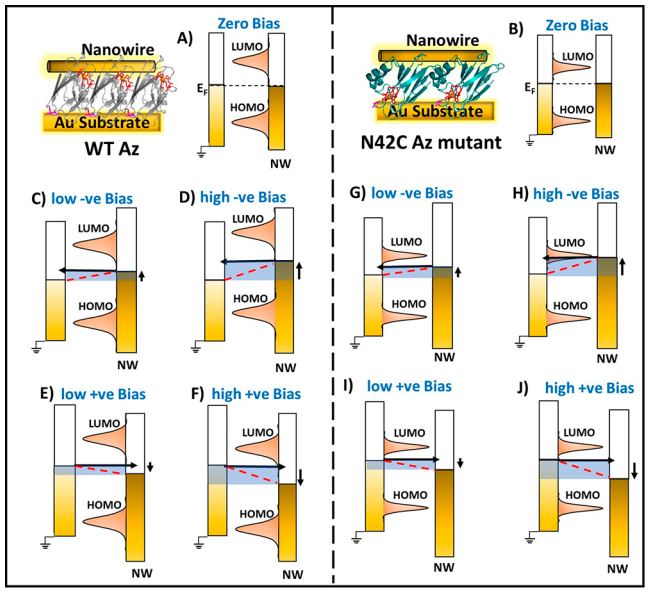

Figure 6. Qualitative energy level schemes for solid-state Az junctions. (A, B) Energy level diagram of Au−*WT Az*−Au and Au−*N42C Az*−Au, respectively, at zero bias. The position of the Lorentzian (shown in pale orange) indicates the electrode to which the Cu(II) cocoordination energy levels are pinned. For *WT Az* (A) the energy levels are pinned to the AuNW, and for the *N42C Az* mutant (B) the energy levels are pinned to the bottom Au electrode. (C, D, E, and F) Au−*WT Az*−Au and (G, H, I, and J) Au−*N42C Az*−Au corresponding junction. (C and E) *WT Az* junction at <|0.5| V bias; (D and F) As C and E, but at higher (negative and positive) bias (>|0.8| V). For *WT Az* junctions only off-resonant tunneling occurs, because the protein energy levels are pinned to the NW Au electrode. (G, I) *N42C Az* junction at <|0.5| V bias, consistent with off-resonant tunneling transport. (H) At higher negative bias, <−0.8 V, the horizontal black arrow indicates on-resonant tunneling. (J) At higher positive bias, >+0.8 V, consistent with off-resonant tunneling, because at zero bias |HOMO-E_f| > |LUMO-E_f|, where HOMO and LUMO refer to the centers of those levels.

The junctions' stability and the reproducibility of our measurements were further checked by back-and-forth scanning of multiple different samples, prepared on different days, as well as by checking several junctions made of each sample (see Figure 3C and F). The bias at which the conductance switch was observed could vary slightly among the experiments, from junction to junction, probably due to the variations in the orientation of the protein (see SI Figure S8).

We plan to look further into computational analysis of the orientation of Az, attached via a Au−S bond to a Au surface, as was done earlier for WT-Az and different types of single amino-acid Az mutants.[37,38] Although these calculations can provide useful information, they are highly time-demanding and beyond the scope of the present study.

Ultraviolet Photoelectron Spectroscopic Data. Details of the complex interfacial electronic structure, including the possible shift of the vacuum level at the protein−electrode interface, were investigated by ultraviolet photoelectron spectroscopy (UPS) measurements. The work functions (W_f) of the surface-bound *N42C Az* and *WT Az* proteins were obtained from the high secondary electron photoemission cutoff (SEPC), where $W_f = h\nu$ − SEPC, with $h\nu$ the energy of the UV photon source (HeI line) = 21.22 eV. As shown in Figure 5A, SEPC values differ between surfaces covered with a monolayer of *WT* and *N42C Az* by ∼0.3 eV, reflecting the sensitivity of the W_f of a surface to its chemical composition. A (relatively) clean Au surface (W_f = 5.0 eV) served to obtain a reference energy level (see Figure 5A).

Modification of the Au surface with the proteins decreased the work function, by ∼0.4 eV for the *N42C Az* monolayer and by ∼0.7 eV for *WT Az* (Figure 5A). These W_f decreases mean that the surfaces become less negative/more positive upon protein adsorption, which is reasonable, because of cancellation of the spillover electron density from the clean Au (pillow effect; cf. ref 39); the ∼0.3 eV difference could originate from the positive surface charge at the north pole of Az (proximal to the Cu(II) and its coordination shell). This north pole area serves as the contact surface of the *WT Az*, which has therefore the smallest W_f. In addition, there could be some differences in charge redistribution between the two protein mutants and the Au substrate at the interface, which can affect what is otherwise a pure dipole effect.

Even though both types of Az are bound to the Au substrate via Au−S bonds, the proximity of the electron-rich Cu(II) and its coordination shell to the Au−S substrate bond should make the substrate−protein coupling for the *N42C Az* stronger than for the *WT Az*, with a possible enhanced charge redistribution. All other factors being equal, in the tight-binding/molecular orbital models, stronger coupling should increase the energy difference between both the HOMO (assuming it is bonding) and LUMO (assuming it is antibonding) and the Fermi level (reflected by the W_f). How then can the measured onsets of the UPS signal yield an opposite result (Figure 5B)? The reason is that the UPS measurements are carried out *without the second contact*, the AuNW. It is conceivable that the interaction between the AuNW and the surface proximal Cu(II) coordination shell of *WT Az* will modify the surface

https://dx.doi.org/10.1021/jacs.0c08836
J. Am. Chem. Soc. 2020, 142, 19217−19225

energetics (for more details, please see the Discussion). Here we identify this low bond energy photoemission onset with the higher occupied molecular orbital (HOMO) of the material from which the first electronic transition takes place. A clear Au surface was used for the determination of the Fermi level position (E_f) of the instrument (sample), where, according to definition,[40] the binding energy is equal to zero (E_f = 0 eV). The results shown in Figure 5B indicate that the HOMO onset for the *N42C Az* monolayer is approximately ∼1 eV closer to the electrode Fermi level relative to that of *WT Az*. A zoom-in UPS spectrum of the near E_f range in the semilog scale as well as full-range He I and He II spectra are presented in SI Figures S12 and S13.

DISCUSSION

Electric current conduction via a protein was found to depend on its chemical nature and structure[15,41,42] as well as on the electrode−protein coupling.[18,43,44] To analyze and understand the observed differences in ETp between the *N42C Az* mutant and *WT Az*, we first consider their structural[37,42] and other biophysical properties.[24,45,27] Although substitution by alanines of the two cysteines Cys3 and Cys26, which form the disulfide bond in the *WT Az*, eliminates this bridge, it was found to have a rather limited impact on the mutant's three-dimensional structure.[30,24,27,29] The 3D structure of *N42C Az* shows that the positions of the cysteine 42 Cβ carbons are virtually the same as those of the asparagine Cβ carbons in the *WT* protein.[25]

We next consider the coupling between the protein's frontier molecular orbital energies and the electrodes' energy levels relative to the Fermi level.[22,43] In the SI (Section 10) we use a simple model to estimate these energies and energy levels, by fitting the *I*−*V* curves to a one energy level Landauer model.[46] The results show that in the low-bias (<|0.5 V|) range, over which the fit is possible, coupling of the mutant to the electrodes is a few times stronger than that of the WT. This result rationalizes the observed higher currents, also in this range, where transport is consistent with off-resonant tunneling, even though the effective barriers, derived from the model, are similar.

Stronger electrode−protein coupling leads to stronger electronic inductive effects,[47] which broaden the frontier orbital energy levels and also shift them further away from the electrodes' Fermi levels. Indeed, upon protein binding we observe a clear HOMO onset shift. That shift can be ascribed to orbital hybridization between the Au substrate and the protein. This effect is expected to be stronger for *N42C* than for *WT Az* due to the spatial proximity of the Cu(II) and its electron-rich coordination shell to the bottom Au substrate for *N42C Az*. Such a hybridization process was found for example by computations of a tetra-heme protein[48] interaction with a Au substrate. Naturally, the second contact, with the AuNW, can also modify the surface energetics. A stronger effect is now expected for the *WT Az*, where the Cu(II) and its coordination shell are in close proximity to the AuNW electrode, while the *N42C Az* surface contacts the top AuNW with nonaromatic amino acids. One could thus argue that the end result should be similar energetics for both types of azurins. However, our previous studies of *WT Az*[6] and others of nonprotein molecules[49] show that the energetics of a given junction are dominated mainly by coupling to the electrode to which the protein is chemically bound. This is here the bottom Au electrode, which Papp et al.[50] call the "strong" contact. In our case this is also the contact having by far the largest area, which will reduce any constriction resistance and, thus, also the contact resistance at the contact. Thus, the UPS results provide a fair, even if only rough, possible rationale for the differences in the behavior of the two protein variants. At the same time, the stronger coupling to and hybridization with one of the electrodes make it more likely that the protein energy levels will be pinned to those of that electrode. Indeed, the ETp results are consistent with some protein−electrode energy level pinning.

What will then the energetics of the process have to be in order to bring *N42C Az* in and out of resonance and why is such behavior not observed for *WT Az*? Charge transport by OFF-resonant tunneling[22] may take place under low bias when the energy gaps between the relevant energy levels are on the order of several dozen kTs. "ON-resonant" tunneling becomes possible when the applied bias window is aligned with the Fermi level of one of the electrodes. This is evidenced by a step in the observed current−voltage curve[18,46] and by a peak in the conductance−voltage response plot.[7,18,22] ON-resonant tunneling is rarely observed in conductance measurements via solid-state metal−molecule−metal junctions. The reason for that is possibly associated with the nature of most types of such junctions, which is too delicate to withstand the bias voltages that allow such a transport mechanism. Still, this is often observed in STM measurements.[16,51,52]

The energy level profile of the present studied systems is illustrated in Figure 6 and explained further below. We suggest that the observed differences in ETp reflect the different contacts and orientation of the *WT* and *N42C Az* with, and relative to, the electrodes. Earlier studies have already implicated the Cu(II) coordination shell role in ETp via *WT Az*.[18,20] Both *WT* and the *N42C Az* are bound to the bottom Au electrode by a Au−S bond. However, while for *WT Az* this binding occurs at the opposite, i.e., the protein south end, namely, distant from the Cu(II) coordination shell, the *N42C Az* mutant is bound, via its C42, proximal to that shell, making quite different interactions with the electrodes: The bottom substrate Au electrode is connected to the Cu(II) coordination site of the *N42C Az* mutant via a relatively short set of covalent peptide bonds (Au−S···Cys42···His46[45]), rather than via the ∼1.8 nm long matrix of predominantly beta-sheet protein in *WT Az*. This pins the energy levels of the Cu(II) coordination shell in *N42C Az* mutant to the bottom Au substrate (see Figure 6B).

While Au−S bonds are often called covalent, in fact they are only partially so (<35% was estimated from DFT calculations),[53] which implies some charge localization, important when we compare the *N42C Az*'s close contact to the Cu coordination shell with that of the *WT* protein. In the latter case there is no direct chemical bond linkage, but there is close physical contact between the immediate north end surface of the Cu coordination shell and the AuNW.[18] This physical contact increases the probability of wave function overlap between the Cu(II) coordination orbitals and the top AuNW electrode, resulting in the broadening of the energy levels close to the E_F of the electrodes, including levels of Cu(II) and its coordination shell. In contrast, the electronic energy levels of the *N42C Az* Cu(II) coordination shell are not perturbed by the interaction with the top AuNW electrode. In summary, the Cu(II) coordination shell is more insulated from the top AuNW electrode by the peptide matrix in *N42C Az* than in *WT Az*, weakening its coupling to the latter. This conclusion is

https://dx.doi.org/10.1021/jacs.0c08836
J. Am. Chem. Soc. 2020, 142, 19217−19225

supported by the experimentally observed 2-fold higher resistance observed for *WT Az* than for *N42C Az* over the low bias voltage range, where the *I*−*V* curve is close to linear (around 0.1−1 GΩ·nm^2). This result implies that the mutant's Au−S bonding at a Cu(II) proximal, well-connected locus helps transport more than the *WT*'s Au−S bonding at the south, Cu(II) distal protein's end and that the proximity of the Cu(II) coordination shell surface physical contact to the AuNW of the *WT Az* cannot balance it.

Our interpretation is also in line with that of our earlier results, showing that the energy levels of the protein's frontier orbitals in an Au(substrate)−*WT Az*−AuNW junction are pinned to the AuNW electrode.[18,22] The pinning can be rationalized by the close proximity between the AuNW and the Cu(II) site. Therefore, an external bias, applied to the AuNW electrode, shifts these energy levels together with the AuNW bands as shown in Figure 6E and F, for low and higher bias. Earlier[18] we further showed that separating the Az north pole from the AuNW by a nonconjugated hydrocarbon linker led to bias-induced resonance-like ETp, which was interpreted as result of the reduced electrode and protein coupling. Therefore, to examine the effect of orientation on charge transport via proteins in the solid state, direct attachment of the protein to the Au surface via a Au−S bond is preferable. Moreover, introducing a linker will also affect the protein's orientation by increasing its freedom of movement.

Conductance switching is observed in *N42C Az* only by increasing the negative bias (see Figures 4B, S7), indicating that the Au−*N42C Az*−Au junction is electrically asymmetric. Apart from the asymmetry of the HOMO and LUMO with respect to the electrode's Fermi level (as can be deduced from Figure 5B and illustrated in Figure 6), the protein's intrinsic dipole can make the applied bias drop unequally at the two electrode interfaces. Unequal bias drop can also be a result of the different electrode areas.

In the absence of applied bias voltage, the Fermi energy levels (E_f) of the Au nanowire and the bottom Au substrate are aligned. Figure 6G and I illustrate a schematic energy level diagram of *N42C Az* for applied bias < |0.5| V; 6H at more negative bias >0.8 V; and 6J at more positive bias >0.8 V. For the sake of clarity, we only focus on the LUMO. Our previous transistor experiments on *WT Az* enabled us to deduce that the leading tail of the LUMO is close to the Au Fermi level.[6] When the frontier orbital is located far from the Fermi level, the conductance is low due to being off-resonant tunneling. Upon increasing the applied bias to a more negative value, >0.8 V, the energy levels are shifted and are aligned within the bias window, resulting in resonant tunneling with a rather abrupt, almost 10-fold increase in the conductance. Figure 6C and E illustrate the case for *WT Az*, at low (<|0.5| V) bias, and Figure 6D and F show that at higher bias (>|0.8| V). It appears that the energy levels in both cases are not aligned with the bias window. Therefore, the condition for ON-resonant ETp is not met.

Temperature-independent ETp over long distances constantly challenges the existing ETp models that are used commonly to interpret and analyze experimental data. A major question that is frequently raised is if the observed temperature-independent ETp over long distances is really due to quantum mechanical tunneling? ETp measurements carried out on a protein junction rely completely on examining their temperature dependence for understanding their mechanism, given that hitherto reliable thickness dependence measurements are hard to impossible on a given protein molecule. Our current finding that the use of protein−electrode orientation manipulation and its control can push the system energy levels in and out of resonant tunneling by varying the applied bias provides an important indirect measurement of quantum mechanical tunneling in action. This result is most relevant to the fundamental understanding of ETp via proteins. It also suggests a novel strategy for regulating conductance switching by controlling protein−electrode orientation.

CONCLUSION

We observe, reproducibly, a marked increase in conductance (up to 10-fold, showing a conductance peak) at negative bias via Au−*N42C Az*−Au junctions, which is interpreted as being a direct OFF- to ON-resonant charge tunneling transition. This remarkable observation became possible because the *N42C Az* is partly decoupled from one of the electrodes. Importantly, the junction is stable up to ∼|1.2| V. No conductance switching is observed for *WT Az*, where the main difference between the two junctions is the flipped protein orientation with respect to the electrodes and the direct Au−S bond being to one of the electrodes proximal to the protein's redox center. He source-based UPS measurements of the *N42C Az* on Au provide a quantitative rationale for the observed bias-dependent switch. Electrically controlled, solid-state conductance switching of proteins, as presented and rationalized here, is an important step toward potential use of proteins in bioelectronic devices.

ASSOCIATED CONTENT

Supporting Information

The Supporting Information is available free of charge at https://pubs.acs.org/doi/10.1021/jacs.0c08836.

Information related to the materials and methods section, characterization data (PM-IRRAS, UV−vis, and AFM), detailed analysis of XPS results of *N42C* and *WT Az* on the Au surface, reproducibility test, Arrhenius plot, and the UPS data (PDF)

AUTHOR INFORMATION

Corresponding Authors

Jerry A. Fereiro − *Department of Materials and Interfaces, Weizmann Institute of Science, Rehovot 76100, Israel;* Email: jerry.fereiro@weizmann.ac.il

Mordechai Sheves − *Department of Organic Chemistry, Weizmann Institute of Science, Rehovot 76100, Israel;* orcid.org/0000-0002-5048-8169; Email: mudi.sheves@weizmann.ac.il

David Cahen − *Department of Materials and Interfaces, Weizmann Institute of Science, Rehovot 76100, Israel;* orcid.org/0000-0001-8118-5446; Email: david.cahen@weizmann.ac.il

Authors

Tatyana Bendikov − *Department of Chemical Research Support, Weizmann Institute of Science, Rehovot 76100, Israel*

Israel Pecht − *Department of Immunology, Weizmann Institute of Science, Rehovot 76100, Israel*

Complete contact information is available at: https://pubs.acs.org/10.1021/jacs.0c08836

https://dx.doi.org/10.1021/jacs.0c08836
J. Am. Chem. Soc. 2020, 142, 19217−19225

Notes

The authors declare no competing financial interest.

■ ACKNOWLEDGMENTS

J.F. thanks the Azrieli Foundation for a postdoctoral fellowship. D.C. and M.S. thank the Israel Science Foundation (ISF), the German Science Foundation (DFG), and the Benoziyo Endowment Fund for the Advancement of Science for partial support. The research is made possible in part by the historic generosity of the Harold Perlman family. M.S. holds the Katzir-Makineni Chair in Chemistry.

■ REFERENCES

(1) Bostick, C. D.; Mukhopadhyay, S.; Pecht, I.; Sheves, M.; Cahen, D.; Lederman, D. Protein bioelectronics: a review of what we do and do not know. *Rep. Prog. Phys.* **2018**, *81* (2), No. 026601.
(2) Alessandrini, A.; Facci, P. Electron transfer in nanobiodevices. *Eur. Polym. J.* **2016**, *83*, 450−466.
(3) Winkler, J. R.; Gray, H. B. Electron flow through metalloproteins. *Chem. Rev.* **2014**, *114* (7), 3369−3380.
(4) Chen, Z. B.; Kibler, R. D.; Hunt, A.; Busch, F.; Pearl, J.; Jia, M. X.; VanAernum, Z. L.; Wicky, B. I. M.; Dods, G.; Liao, H.; Wilken, M. S.; Ciarlo, C.; Green, S.; El-Samad, H.; Stamatoyannopoulos, J.; Wysocki, V. H.; Jewett, M. C.; Boyken, S. E.; Baker, D. De novo design of protein logic gates. *Science* **2020**, *368* (6486), 78.
(5) Wang, H.; Meng, F. B.; Zhu, B. W.; Leow, W. R.; Liu, Y. Q.; Chen, X. D. Resistive Switching Memory Devices Based on Proteins. *Adv. Mater.* **2015**, *27* (46), 7670−7676.
(6) Kayser, B.; Fereiro, J. A.; Guo, C. L.; Cohen, S. R.; Sheves, M.; Pecht, I.; Cahen, D. Transistor configuration yields energy level control in protein-based junctions. *Nanoscale* **2018**, *10* (46), 21712−21720.
(7) Fereiro, J. A.; Kayser, B.; Romero-Muniz, C.; Vilan, A.; Dolgikh, D. A.; Chertkova, R. V.; Cuevas, J. C.; Zotti, L. A.; Pecht, I.; Sheves, M.; Cahen, D. A Solid-State Protein Junction Serves as a Bias-Induced Current Switch. *Angew. Chem., Int. Ed.* **2019**, *58* (34), 11852−11859.
(8) Solomon, E. I.; Hadt, R. G. Recent advances in understanding blue copper proteins. *Coord. Chem. Rev.* **2011**, *255* (7), 774−789.
(9) Solomon, E. I.; Heppner, D. E.; Johnston, E. M.; Ginsbach, J. W.; Cirera, J.; Qayyum, M.; Kieber-Emmons, M. T.; Kjaergaard, C. H.; Hadt, R. G.; Tian, L. Copper Active Sites in Biology. *Chem. Rev.* **2014**, *114* (7), 3659−3853.
(10) Andolfi, L.; Bruce, D.; Cannistraro, S.; Canters, G. W.; Davis, J. J.; Hill, H. A. O.; Crozier, J.; Verbeet, M. P.; Wrathmell, C. L.; Astier, Y. The electrochemical characteristics of blue copper protein monolayers on gold. *J. Electroanal. Chem.* **2004**, *565* (1), 21−28.
(11) Baldacchini, C.; Bizzarri, A. R.; Cannistraro, S., Excitation of the ligand-to-metal charge transfer band induces electron tunnelling in azurin. *Appl. Phys. Lett.* **2014**, *104* (9).
(12) Baldacchini, C.; Bizzarri, A. R.; Cannistraro, S. Electron transfer, conduction and biorecognition properties of the redox metalloprotein Azurin assembled onto inorganic substrates. *Eur. Polym. J.* **2016**, *83*, 407−427.
(13) Pompa, P. P.; Brarnanti, A.; Maruccio, G.; del Mercato, L. L.; Chiuri, R.; Cingolani, R.; Rinaldi, R. Effects of high external electric fields on protein conformation. In *Nanotechnology II*; Lugli, P.; Kish, L. B.; Mateos, J., Eds.; 2005; Vol. *5838*, pp 171−181.
(14) Pompa, P. P.; Bramanti, A.; Maruccio, G.; Mercato, L. L. d.; Cingolani, R.; Rinaldi, R. Ageing of solid-state protein films: Behavior of azurin at ambient conditions. *Chem. Phys. Lett.* **2005**, *404* (1), 59−62.
(15) Ruiz, M. P.; Aragonès, A. C.; Camarero, N.; Vilhena, J. G.; Ortega, M.; Zotti, L. A.; Pérez, R.; Cuevas, J. C.; Gorostiza, P.; Díez-Pérez, I. Bioengineering a Single-Protein Junction. *J. Am. Chem. Soc.* **2017**, *139* (43), 15337−15346.
(16) Chi, Q. J.; Farver, O.; Ulstrup, J. Long-range protein electron transfer observed at the single-molecule level: In situ mapping of redox-gated tunneling resonance. *Proc. Natl. Acad. Sci. U. S. A.* **2005**, *102* (45), 16203−16208.
(17) Chi, Q. J.; Zhang, J. D.; Andersen, J. E. T.; Ulstrup, J. Ordered assembly and controlled electron transfer of the blue copper protein azurin at gold (111) single-crystal substrates. *J. Phys. Chem. B* **2001**, *105* (20), 4669−4679.
(18) Fereiro, J. A.; Yu, X.; Pecht, I.; Sheves, M.; Cuevas, J. C.; Cahen, D. Tunneling explains efficient electron transport via protein junctions. *Proc. Natl. Acad. Sci. U. S. A.* **2018**, *115* (20), E4577−E4583.
(19) Alessandrini, A.; Salerno, M.; Frabboni, S.; Facci, P. Single-metalloprotein wet biotransistor. *Appl. Phys. Lett.* **2005**, *86* (13),133902.
(20) Amdursky, N.; Sepunaru, L.; Raichlin, S.; Pecht, I.; Sheves, M.; Cahen, D. Electron transfer proteins as electronic conductors: Significance of the metal and Its binding site in the blue Cu protein, azurin. *Adv. Sci.* **2015**, *2* (4).
(21) Artes, J. M.; Diez-Perez, I.; Sanz, F.; Gorostiza, P. Direct Measurement of Electron Transfer Distance Decay Constants of Single Redox Proteins by Electrochemical Tunneling Spectroscopy. *ACS Nano* **2011**, *5* (3), 2060−2066.
(22) Fereiro, J. A.; Porat, G.; Bendikov, T.; Pecht, I.; Sheves, M.; Cahen, D. Protein Electronics: Chemical Modulation of Contacts Control Energy Level Alignment in Gold-Azurin-Gold Junctions. *J. Am. Chem. Soc.* **2018**, *140* (41), 13317−13326.
(23) Mukhopadhyay, S.; Karuppannan, S. K.; Guo, C.; Fereiro, J. A.; Bergren, A.; Mukundan, V.; Qiu, X.; Castañeda Ocampo, O. E.; Chen, X.; Chiechi, R. C.; McCreery, R.; Pecht, I.; Sheves, M.; Pasula, R. R.; Lim, S.; Nijhuis, C. A.; Vilan, A.; Cahen, D. Solid-state protein charge transport: cross-laboratory study shows preservation of transport mechanism, with electronic coupling dictating efficiency. *iScience* **2020**, *23*, 101099.
(24) van Amsterdam, I. M. C.; Ubbink, M.; Jeuken, L. J. C.; Verbeet, M. P.; Einsle, O.; Messerschmidt, A.; Canters, G. W. Effects of dimerization on protein electron transfer. *Chem. - Eur. J.* **2001**, *7* (11), 2398−2406.
(25) van Amsterdam, I. M. C.; Ubbink, M.; Einsle, O.; Messerschmidt, A.; Merli, A.; Cavazzini, D.; Rossi, G. L.; Canters, G. W. Dramatic modulation of electron transfer in protein complexes by crosslinking. *Nat. Struct. Biol.* **2002**, *9* (1), 48−52.
(26) Ambler, R. P.; Brown, L. H. The amino acid sequence of Pseudomonas fluorescens azurin. *Biochem. J.* **1967**, *104* (3), 784−825.
(27) Farver, O.; Pecht, I. Long-range intramolecular electron-transfer in azurins. *Proc. Natl. Acad. Sci. U. S. A.* **1989**, *86* (18), 6968−6972.
(28) Guzzi, R.; Milardi, D.; La Rosa, C.; Grasso, D.; Verbeet, M. P.; Canters, G. W.; Sportelli, L. The effect of copper/zinc replacement on the folding free energy of wild type and Cys3Ala/Cys26Ala azurin. *Int. J. Biol. Macromol.* **2003**, *31* (4), 163−170.
(29) Guzzi, R.; Sportelli, L.; La Rosa, C.; Milardi, D.; Grasso, D.; Verbeet, M. P.; Canters, G. W. A Spectroscopic and Calorimetric Investigation on the Thermal Stability of the Cys3Ala/Cys26Ala Azurin Mutant. *Biophys. J.* **1999**, *77* (2), 1052−1063.
(30) Bonander, N.; Leckner, J.; Guo, H.; Karlsson, B. G.; Sjölin, L. Crystal structure of the disulfide bond-deficient azurin mutant C3A/C26A. *Eur. J. Biochem.* **2000**, *267* (14), 4511−4519.
(31) Yu, X.; Lovrincic, R.; Sepunaru, L.; Li, W.; Vilan, A.; Pecht, I.; Sheves, M.; Cahen, D. Insights into solid-state electron transport through proteins from inelastic tunneling spectroscopy: The case of azurin. *ACS Nano* **2015**, *9* (10), 9955−9963.
(32) Smith, P. A.; Nordquist, C. D.; Jackson, T. N.; Mayer, T. S.; Martin, B. R.; Mbindyo, J.; Mallouk, T. E. Electric-field assisted assembly and alignment of metallic nanowires. *Appl. Phys. Lett.* **2000**, *77* (9), 1399−1401.
(33) Freer, E. M.; Grachev, O.; Duan, X. F.; Martin, S.; Stumbo, D. P. High-yield self-limiting single-nanowire assembly with dielectrophoresis. *Nat. Nanotechnol.* **2010**, *5* (7), 525−530.
(34) Kayser, B.; Fereiro, J. A.; Bhattacharyya, R.; Cohen, S. R.; Vilan, A.; Pecht, I.; Sheves, M.; Cahen, D. Solid-State Electron Transport via

https://dx.doi.org/10.1021/jacs.0c08836
J. Am. Chem. Soc. 2020, 142, 19217−19225

the Protein Azurin is Temperature-Independent Down to 4 K. *J. Phys. Chem. Lett.* **2020**, *11* (1), 144−151.
(35) Li, W. J.; Sepunaru, L.; Amdursky, N.; Cohen, S. R.; Pecht, I.; Sheves, M.; Cahen, D. Temperature and force dependence of nanoscale electron transport via the Cu protein azurin. *ACS Nano* **2012**, *6* (12), 10816−10824.
(36) Pompa, P. P.; Bramanti, A.; Maruccio, G.; Cingolani, R.; De Rienzo, F.; Corni, S.; Di Felice, R.; Rinaldi, R. Retention of nativelike conformation by proteins embedded in high external electric fields. *J. Chem. Phys.* **2005**, *122* (18), 181102.
(37) Romero-Muñiz, C.; Ortega, M.; Vilhena, J. G.; Diéz-Pérez, I.; Cuevas, J. C.; Pérez, R.; Zotti, L. A. Mechanical Deformation and Electronic Structure of a Blue Copper Azurin in a Solid-State Junction. *Biomolecules* **2019**, *9* (9), 506.
(38) Ortega, M.; Vilhena, J. G.; Zotti, L. A.; Díez-Pérez, I.; Cuevas, J. C.; Pérez, R. Tuning Structure and Dynamics of Blue Copper Azurin Junctions via Single Amino-Acid Mutations. *Biomolecules* **2019**, *9* (10), 611.
(39) Kahn, A. Fermi level, work function and vacuum level. *Mater. Horiz.* **2016**, *3* (1), 7−10.
(40) Norsko, J. K. Chemisorption on metal surfaces. *Rep. Prog. Phys.* **1990**, *53* (10), 1253−1295.
(41) Ron, I.; Sepunaru, L.; Itzhakov, S.; Belenkova, T.; Friedman, N.; Pecht, I.; Sheves, M.; Cahen, D. Proteins as electronic materials: Electron transport through solid-state protein monolayer junctions. *J. Am. Chem. Soc.* **2010**, *132* (12), 4131−4140.
(42) Kumar, K. S.; Pasula, R. R.; Lim, S.; Nijhuis, C. A. Long-range tunneling processes across ferritin-based Junctions. *Adv. Mater.* **2016**, *28* (9), 1824−1830.
(43) Liu, Z. F.; Neaton, J. B. Voltage Dependence of Molecule-Electrode Coupling in Biased Molecular Junctions. *J. Phys. Chem. C* **2017**, *121* (39), 21136−21144.
(44) Amdursky, N.; Ferber, D.; Bortolotti, C. A.; Dolgikh, D. A.; Chertkova, R. V.; Pecht, I.; Sheves, M.; Cahen, D. Solid-state electron transport via cytochrome C depends on electronic coupling to electrodes and across the protein. *Proc. Natl. Acad. Sci. U. S. A.* **2014**, *111* (15), 5556−5561.
(45) Farver, O.; Canters, G. W.; van Amsterdam, I.; Pecht, I. Intramolecular Electron Transfer in a Covalently Linked Mutated Azurin Dimer. *J. Phys. Chem. A* **2003**, *107* (35), 6757−6760.
(46) Cuevas, J. C.; Scheer, E. *Molecular Electronics: An Introduction to Theory and Experiment*; World Scientific, 2017; Vol. *1*.
(47) Sayed, S. Y.; Fereiro, J. A.; Yan, H. J.; McCreery, R. L.; Bergren, A. J. Charge transport in molecular electronic junctions: Compression of the molecular tunnel barrier in the strong coupling regime. *Proc. Natl. Acad. Sci. U. S. A.* **2012**, *109* (29), 11498−11503.
(48) Futera, Z.; Ide, I.; Kayser, B.; Garg, K.; Jianga, X.; van Wonderen, J. H.; Butt, J. N.; Ishii, H.; Pecht, I.; Sheves, M.; Cahen, D.; Blumberger, J. Off-resonant coherent electron transport over three nanometers in multi-heme protein bioelectronic junctions. In revision.*In Revision*
(49) Fereiro, J. A.; McCreery, R. L.; Bergren, A. J. Direct Optical Determination of Interfacial Transport Barriers in Molecular Tunnel Junctions. *J. Am. Chem. Soc.* **2013**, *135* (26), 9584−9587.
(50) Papp, E.; Jelenfi, D. P.; Veszeli, M. T.; Vattay, G. A Landauer Formula for Bioelectronic Applications. *Biomolecules* **2019**, *9* (10), 599.
(51) Frascerra, V.; Calabi, F.; Maruccio, G.; Pornpa, P. P.; Cingolani, R.; Rinaldi, R. Resonant electron tunneling through azurin in air and liquid by scanning tunneling microscopy. *Ieee Transactions on Nanotechnology* **2004**, *4* (5), 637−640.
(52) Facci, P.; Alliata, D.; Cannistraro, S. Potential-induced resonant tunneling through a redox metalloprotein investigated by electrochemical scanning probe microscopy. *Ultramicroscopy* **2001**, *89* (4), 291−298.
(53) Pakiari, A. H.; Jamshidi, Z. Nature and Strength of M−S Bonds (M = Au, Ag, and Cu) in Binary Alloy Gold Clusters. *J. Phys. Chem. A* **2010**, *114* (34), 9212−9221.

https://dx.doi.org/10.1021/jacs.0c08836
J. Am. Chem. Soc. 2020, 142, 19217−19225